

Twelve sublattice ordered phase in the $J_1 - J_2$ model on the kagomé lattice

J.-C. Domenge,* P. Sindzingre, and C. Lhuillier
*Laboratoire de Physique Théorique de la Matière Condensée,
 CNRS UMR 7600, Université Pierre et Marie Curie,
 Boîte Postale 121, 4, place Jussieu, 75252 Paris Cedex, France*

L. Pierre
Batiment G, Université Paris-X, Nanterre, 92001 Nanterre Cedex, France
 (Dated: November 22, 2018)

Motivated by recent experiments on an $S = 1/2$ antiferromagnet on the kagomé lattice, we investigate the Heisenberg $J_1 - J_2$ model with ferromagnetic J_1 and antiferromagnetic J_2 .

Classically the ground state displays Néel long range order with 12 non-coplanar sublattices. The order parameter has the symmetry of a cuboctahedron, it fully breaks $SO(3)$ as well as the spin-flip symmetry, and we expect from the latter a \mathbb{Z}_2 symmetry breaking pattern. As might be expected from the Mermin-Wagner theorem in two dimensions, the $SO(3)$ symmetry is restored by thermal fluctuations while the \mathbb{Z}_2 symmetry breaking persists up to a finite temperature.

A complete study of $S = 1/2$ exact spectra reveals that the classical order subsists for quantum spins in a finite range of parameters. First order spin wave calculations give the range of existence of this phase and the renormalisations at $T = 0$ of the order parameters associated to both symmetry breakings. This phase is destroyed by quantum fluctuations for a small but finite $J_2/|J_1| \simeq 3$, consistently with exact spectra studies which indicate a gapped phase.

I. THEORETICAL AND EXPERIMENTAL ISSUES

Whatever the nature of the spin, classical or quantum, the first neighbor Heisenberg antiferromagnet on the kagomé lattice fails to display Néel-like long range order. Classically, it is characterized by an extensive entropy^{1,2} at $T = 0$. Quantum mechanically the spin-1/2 system has an exceptionally large density of low lying excitations^{3,4} reminiscent of the classical extensive entropy. It is still debated whether and eventually how this degeneracy is lifted in the quantum limit^{5,6}.

An essential issue concerns the influence of perturbations: classically the effect of a second neighbor coupling J_2 has been very early studied by Harris and co-workers⁷. They showed that an infinitesimal J_2 is sufficient to drive the system towards an ordered phase with the three spins around a triangle pointing at 120° from each other. Antiferromagnetic second-neighbor coupling ($J_2 > 0$) favors the $\mathbf{q} = \mathbf{0}$ Néel order of this pattern on the Bravais lattice, whereas there are nine spins per unit cell for $J_2 < 0$ ($\mathbf{q} = \sqrt{3} \times \sqrt{3}$ order). The effect of Dzyaloshinsky-Moriya interactions has also been analysed⁸. To our knowledge the reduction of the order parameter by quantum fluctuations has only been studied through exact diagonalizations⁹. This approach points to an immediate transition from the "disordered phase" at the pure $J_1 > 0$ point, to the semi-classical Néel phases.

Up to now the $J_1 - J_2$ model on the kagomé lattice has only been studied for antiferromagnetic J_1 . Many magnetic compounds^{10–13}, with this geometry, have been studied so far, but most of them have spin $S = 3/2$. A few compounds with $S = 1/2$ Cu ions have recently been

synthesized^{14–16}. None of them can be described by a pure isotropic, first neighbor antiferromagnetic Heisenberg model. Recent experimental work on an organic compound with copper ions on a kagomé lattice¹⁷ gives indication of competing ferromagnetic and antiferromagnetic interactions.

It is thus the purpose of the present work to extend the previous study of the $J_1 - J_2$ model to ferromagnetic nearest neighbor coupling ($J_1 < 0$). The Hamiltonian reads:

$$\mathcal{H} = J_1 \sum_{\langle i,j \rangle} \mathbf{S}_i \cdot \mathbf{S}_j + J_2 \sum_{\langle\langle i,k \rangle\rangle} \mathbf{S}_i \cdot \mathbf{S}_k \quad (1)$$

where the first and second sums run respectively over pairs of nearest neighbors $\langle i,j \rangle$ and next-nearest neighbors $\langle\langle i,k \rangle\rangle$.

For a pure ferromagnetic $J_1 < 0$ coupling the system is indeed in a ferromagnetic phase. For a pure antiferromagnetic second neighbor interaction the model reduces to three decoupled kagomé lattices with antiferromagnetic interactions, and has thus an extensive entropy in the classical limit. The behavior of the model between this two limits is the object of the present study.

In section II the classical ground state of the Hamiltonian (1) is investigated and the phase diagram of the model is given in the classical limit. For competing interactions $J_1 < 0$ and $J_2 > 0$ the model exhibits an ordered phase with 12 sublattices which fully breaks $SO(3)$ as well as a discrete symmetry (chiral symmetry breaking). We show that contrary to the Néel order, which breaks a continuous symmetry and therefore is destroyed down to infinitesimal temperatures, the chiral order survives thermal fluctuations and undergoes a phase transition at finite temperature.

In section III we study the $S = 1/2$ quantum model us-

ing exact diagonalizations and show the premise of the semi-classical ordering on samples up to 36 spins. In section IV we study the effect of long wavelength quantum fluctuations on this semi-classical order in the spin-wave approximation. It appears that the twelve sublattice Néel order survives quantum fluctuations in an extended range of parameters but is destroyed for a non zero $J_2 > 0$ ($J_2/|J_1| \gtrsim 3$). In section V we show that exact diagonalizations in this range of parameters indeed point to (a) gapped phase(s).

II. CLASSICAL APPROACH

In this section we restrict ourselves to classical spins: the spins \mathbf{S}_i are usual unit vectors living in a three-dimensional space.

A. Ground state for $J_1 < 0$ and $J_2 > |J_1|/3$

To investigate the nature of the ground state of the Hamiltonian (1) we first Fourier-transform it to find its lowest-energy modes. The kagomé lattice having three sites per Bravais cell we get three branches. For $J_1 < 0$ and $J_2 < 0$ we find a single minimum at $\mathbf{q} = \mathbf{0}$ corresponding to the expected ferromagnetic ground state. Upon increasing $J_2 > 0$ we find three degenerate minima at the edge centers of the first Brillouin zone, the classical transition occurring at $J_2 = |J_1|/3$. The three modes $\mathbf{q} = \mathbf{X}_{1,2,3}$ (Fig. 1) are the only solution as long as $J_2 > |J_1|/3$ and in the limit of pure $J_2 > 0$ one recovers the flat zero-energy branch of the pure $J_1 > 0$ case: we then have three decoupled kagomé lattices with nearest neighbor coupling J_2 . In the $J_1 < 0$, $J_2 > |J_1|/3$ re-

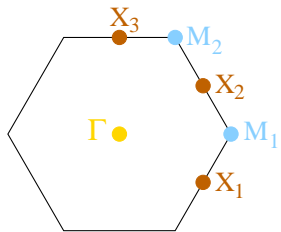


FIG. 1: (Color online) First Brillouin zone of the kagomé lattice with its points of high symmetry: the center of zone Γ ($\mathbf{q} = \mathbf{0}$), the two zone corners M_1 and M_2 and the three edge centers X_1 , X_2 and X_3 .

gion the unit cell compatible with the three edge centers contains 12 sites and the direct minimization of (1) for small samples of size multiple of 12 indeed reveals a Néel long-range order with 12 non-coplanar sublattices pointing towards the 12 centers of edges of a cube (Fig. 2). The apparent complexity of this structure is somewhat enlightened when one considers the six spins around an hexagon: they lie in the same plane and make an angle

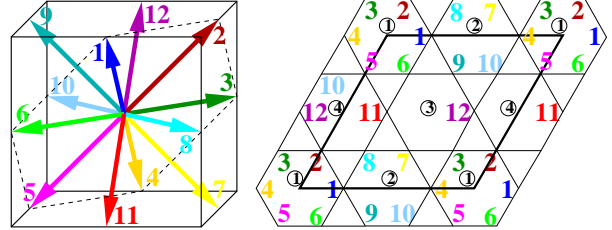


FIG. 2: (Color online) Classical order parameter for $J_1 < 0$ and $J_2 > |J_1|/3$ with the associated lattice symmetry breaking. The twelve sublattices and the four different types of hexagons are numbered. Also shown is the plane containing the six spins of hexagon 1 (dashed).

$\pi/3$ with their nearest neighbours. We thus have four hexagons in the unit cell defining four different planes oriented like the faces of a tetrahedron. The polyhedron whose vertices coincide with the directions of the sublattices is named a cuboctahedron and we will refer to that order parameter as the *cuboc* phase in the following. Consistently, Monte-Carlo simulations with a Metropolis algorithm reveal a local *cuboc* Néel order with fluctuations increasing with temperature.

We now have a complete picture of the classical phase diagram of the Hamiltonian (1) at $T = 0$ in the entire $J_1 - J_2$ plane (Fig. 3).

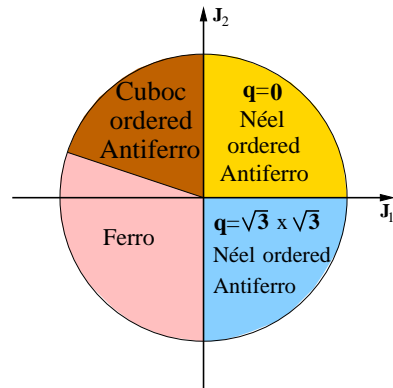


FIG. 3: (Color online) Classical phase diagram of the Heisenberg $J_1 - J_2$ model on the kagomé lattice at $T = 0$. The transition between the ferromagnetic state and the antiferromagnetic *cuboc* state occurs at $J_2 = -J_1/3$.

B. Discrete symmetry breaking

It is clear that $O(3)$ is fully broken in the *cuboc* phase at $T = 0$: the point group symmetry of a cuboctahedron is simply that of the cube, *i.e.* $\mathcal{O}_h = \mathcal{O} \times \{Id, i\}$, where \mathcal{O} is the octahedral group containing the 24 rotations leaving a cube or an octahedron invariant, and Id and i are respectively the identity and the spin-inversion, or

spin-flip.

An important result arises when one considers the action of the spin-flip alone. It is clear that i acting on a cuboctahedron takes it onto another cuboctahedron, but the labels of the two cuboctahedra can't be made to coincide by means of a global rotation. Namely, the order parameter we obtain is the mirror-symmetry image of the previous one (Fig. 4). The order parameter in the

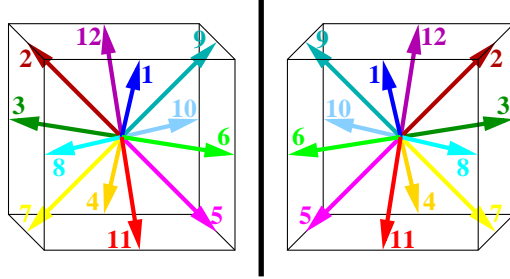


FIG. 4: (Color online) An order parameter and its image by a spin-flip. After a global rotation of the sublattice directions it is clear that the two order parameters are related one to the other by a mirror symmetry.

cuboc phase thus breaks the spin-flip symmetry and we are able to divide the ground states manifold into two classes. This makes us expect a transition at finite temperature associated to this \mathbb{Z}_2 symmetry breaking.

To show that this is indeed the case we define a variable labelling the two classes of ground states. Consider the normalised scalar chirality on a triangle, namely $\sigma_\Delta = \frac{(\mathbf{S}_i \wedge \mathbf{S}_j) \cdot \mathbf{S}_k}{\|\mathbf{S}_i \wedge \mathbf{S}_j\| \|\mathbf{S}_k\|}$ with (i,j,k) labelling the three sites clockwise. Inspection of the order parameter of Fig. 2 reveals that σ_Δ is alternatively +1 on upward triangles and -1 on downward triangles (Fig. 5). We naturally define the alternate scalar chirality as

$$m_\sigma = \frac{3}{2N} \sum_{\Delta} (-1)^{\alpha_\Delta} \sigma_\Delta \quad (2)$$

where the sum runs over the $2N/3$ triangles of the kagomé lattice, and α_Δ is respectively 0 and 1 on upward and downward triangles. The spin-flip trivially changes the sign of σ_Δ , so that $m_\sigma = \pm 1$ at zero temperature, depending on the class of the order parameter. Hence, m_σ is the order parameter associated to the spin-flip symmetry breaking.

Monte-Carlo simulations have been performed on samples with up to 1200 spins: they show that m_σ vanishes at finite temperature, while the associated chiral susceptibility, defined as:

$$k_B \chi_\sigma = \frac{2N}{3T} (\langle m_\sigma^2 \rangle - \langle |m_\sigma| \rangle^2) \quad (3)$$

and the specific heat seemingly both diverge (Fig. 6). Typical simulations involved 10^6 Monte-Carlo steps per spin. First results indicate that the transition is not in the

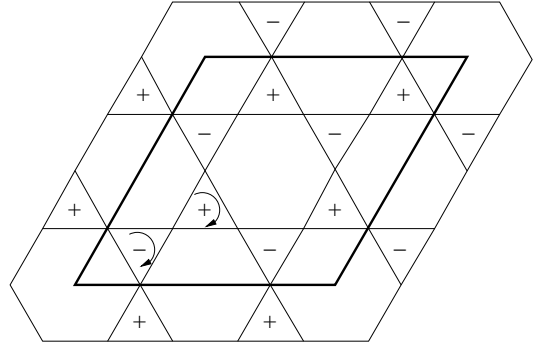


FIG. 5: The normalised scalar chirality σ_Δ computed on the order parameter of figure 2. The spin-flip trivially permutes the + and -.

two-dimensionnal Ising universality class. The complexity of the global set of excitations which does not reduce to those of the above-mentionned σ_Δ variable are probably at the origin of a more complex behavior, presumably a weak first-order phase transition¹⁸. The complete study of this classical phase transition will be published elsewhere¹⁹.

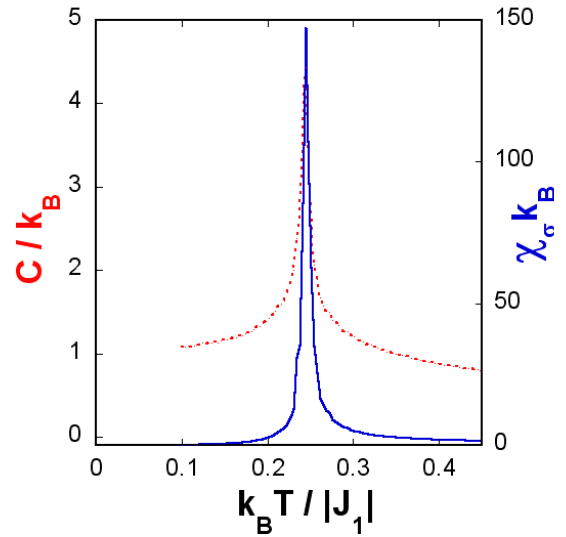


FIG. 6: (Color online) Specific heat C/k_B (red dashed line) and chiral susceptibility $k_B \chi_\sigma$ (blue solid line) vs. temperature on a 1200 spins sample for $J_2/J_1 = 0.5$: both quantities diverge at $T_c = 0.24$, simultaneously with the vanishing of the chiral order parameter m_σ (not shown).

III. SPIN 1/2 MODEL

We now turn to the spin 1/2 quantum model. Considering the classical analysis, the question is whether quantum fluctuations are strong enough to wipe out the classical order. If so, we end up with a purely quantum

phase such as a Valence Bond Solid or a RVB-liquid⁶. If not, this means that quantum fluctuations merely dress the classical order parameter, reducing the mean sublattice magnetization while preserving its symmetries. Such states may thus be referred to as *semi-classical* states.

A. À la Néel $SU(2)$ symmetry breaking

Exact spectra of finite size samples have already been shown to be a powerful tool to find eventual Néel orders in quantum spin systems^{20,21}. Of course they allow for the exact computation of the square of the sublattice magnetization or any relevant structure factor. But mostly, while the extensive use of the symmetries of the Hamiltonian is compulsory in order to diagonalize large enough samples (typically 36 spins today), it also gives a clear signature of $SU(2)$ -breaking phases, even on small samples spectra.

Namely, for an $SU(2)$ symmetry breaking, we expect a large set of low lying eigenstates of the hamiltonian, with different total spin S values, to collapse onto the ground-state when the size of the sample $N \rightarrow \infty$. These states have been called the *quasidegenerate joint states* [QDJS] and they have been recently observed experimentally on nano-magnets²². If the semi-classical picture is valid, these QDJS are expected to have energies well below the magnon excitations and to scale as $S(S+1)/N$ as expected for a quantum top. Exact spectra are thus displayed *vs.* $S(S+1)$ and the QDJS are often referred to as the Anderson's tower of states²³. To have a true $SU(2)$ symmetry breaking in the thermodynamic limit the QDJS should have total spins up to $S \sim \mathcal{O}(\sqrt{N})$. The breaking of the $SU(2)$ symmetry then occurs with all the QDJS collapsing onto the absolute ground state like $1/N$ when $N \rightarrow \infty$, *i.e.* faster than the softest magnons, whose energies scale as $1/\sqrt{N}$, defining the *à la Néel* $SU(2)$ -symmetry breaking scheme²¹. This result explains why it is numerically more favorable to look at the QDJS since order parameters only scale as $1/\sqrt{N}$.

In the thermodynamic limit, the ground state is a superposition of an infinite number of QDJS with different S values, which clearly breaks $SU(2)$.

The crucial point is that in each spin sector the number and symmetries of the QDJS are exactly determined from group representation theory^{3,21} by the symmetry of the expected ground state.

B. Determination of the QDJS

If the thermodynamic ground state exhibits a semi-classical 12-sublattice Néel order then the QDJS, if ever they exist, should be of symmetry compatible with both those of the Hamiltonian (1), since they are eigenstates, and those of the *cuboc* phase, *i.e.* \mathcal{O}_h .

A classical result of group theory is that the number of such states is completely determined by the structures

of the two groups. Indeed, if we restrict ourselves to the rotational symmetry breaking, we see that the original $SO(3)$ symmetry of (1) is reduced to its subgroup \mathcal{O} in the Néel-ordered ground state.

Thus, while D_S is an irreducible representation [IR] of $SO(3)$ of spin S , it is an *a priori* reducible representation of \mathcal{O} that one can decompose onto the five IRs Γ_ν of \mathcal{O} according to

$$D_S = \sum_{\nu=1}^5 n_\nu(S) \Gamma_\nu \quad (4)$$

with

$$n_\nu(S) = \frac{1}{24} \sum_{g \in \mathcal{O}} \chi_\nu^*(g) \chi_S(g) \quad (5)$$

where $\chi_\nu(g)$ and $\chi_S(g)$ are the characters of $g \in \mathcal{O}$ in the IR Γ_ν of \mathcal{O} , and in the IR D_S of $SO(3)$ respectively. The character table of \mathcal{O} is given in Table I and $\chi_S(g) = \frac{\sin((2S+1)\theta/2)}{\sin(\theta/2)}$, with θ the angle of the rotation g . For completeness we give the explicit decomposition (4) for spins up to $S=6$ in Table II.

TABLE I: Character table of \mathcal{O} . Its irreducible representations are named both with the usual nomenclature and with the numbering $1 \leq \nu \leq 5$ used throughout the article. Also shown is the character table of the group $\{Id, i\}$. The character table of the whole \mathcal{O}_h group is obtained by forming the direct product of the two tables.

\mathcal{O}	Id	$8C_3$	$3C_2$	$6C_2$	$6C_4$	ν
A_1	1	1	1	1	1	1
A_2	1	1	1	-1	-1	2
E	2	-1	2	0	0	3
T_1	3	0	-1	-1	1	4
T_2	3	0	-1	1	-1	5

$\{Id, i\}$	Id	i
Γ_e	1	1
Γ_o	1	-1

The decomposition (4) directly gives the number of states that belong both to D_S and Γ_ν , *i.e.* that are compatible with both the $SO(3)$ and \mathcal{O} symmetries, as required for the QDJS. It should be emphasized that for a given S value the number of such states is $n(S) = \sum_{\nu=1}^5 n_\nu(S) \dim \Gamma_\nu = 2S+1$, as expected for a complete $SO(3)$ breaking.

We stress that (4) relies only on group theory and that it makes no reference to the representation space²⁵.

Now, if we are to find the total content of each spin sector of the Anderson's tower of states, we should treat the whole \mathcal{O}_h group, not limiting ourselves to the rotational symmetry breaking $SO(3) \rightarrow \mathcal{O}$ as in (4).

This is particularly simple since \mathcal{O}_h is the direct product of \mathcal{O} with the group $\{Id, i\}$, and the spin-flip being also a symmetry of the Hamiltonian, there is no compatibility issue here. Thus, everytime an IR Γ_ν appears in (4) we actually get two copies of it associated to the two IRs

TABLE II: The decomposition (4) explicated for $S \leq 6$.

$D_0 = A_1$
$D_1 = T_1$
$D_2 = E + T_2$
$D_3 = A_2 + T_1 + T_2$
$D_4 = A_1 + E + T_1 + T_2$
$D_5 = E + 2T_1 + T_2$
$D_6 = A_1 + A_2 + E + T_1 + 2T_2$

of the $\{Id, i\}$ group (Table I). Since these two IRs differ only in their parity under the spin-flip operation, which itself transforms any order parameter into its \mathbb{Z}_2 -image, this double *quasidegeneracy* is clearly reminiscent of the \mathbb{Z}_2 symmetry breaking observed classically.

We thus have formally determined the number and symmetries of the QDJS appearing in each spin sector of the tower of states. However, for a given total spin, their symmetries are given in terms of the IRs of \mathcal{O}_h while exact diagonalizations provide eigenstates of given symmetry under the lattice symmetry group.

It thus remains to map the IRs of \mathcal{O}_h onto those of the lattice symmetry group, namely $G_N = T_N \wedge P_N$, where T_N contains the $N/3$ translations by a Bravais lattice vector and P_N is the point group of the sample (in general P_N is a subgroup of C_{6v} , the point group of the infinite kagomé lattice).

Such a mapping clearly exists since the labelling of the 12 vertices of the cuboctahedron induces a labelling of the lattice (Fig. 2). Applying an element of \mathcal{O}_h to a cuboctahedron means permuting its 12 labels, which itself is equivalent to a lattice transformation.

We thus have a mapping between \mathcal{O}_h and some elements of G_N . Note that while the mapping between the group elements is not necessarily one-to-one, and in fact it is a one-to-many mapping for all the elements of the subgroup \mathcal{O} , the resulting mapping between the IRs of the two groups is one-to-one, as is explicated in Table III.

A notable exception is the spin-flip which is exactly mapped onto the rotation of the lattice R_π by angle π around the center of an empty hexagon. Hence the parity of an eigenstate of the Hamiltonian (1) under R_π is directly equal to its parity under the spin-flip. Thus, if ever the thermodynamic ground state has the classical 12-sublattice structure, we are able to find the number and degeneracies of the expected QDJS using Table II and the one-to-one mapping between the IRs of \mathcal{O}_h and those of G_N (Table III).

However there is still one subtlety. Indeed, in order not to artificially frustrate the 12-sublattice order, we choose samples containing multiples of 12 spins, *i.e.* $N=12, 24$ and 36 spins. The representation spaces of these three samples have different properties since the total spin on each sublattice is $N/24$ which may be integer or half-integer.

To be more specific, we want to write down the matrix $\hat{U}(g) \in SU(2)$ associated to a particular rotation $g \in \mathcal{O}$

TABLE III: One-to-one mapping between the IRs of \mathcal{O}_h and those of G_N . We considered a sample having the three edge centers in its first Brillouin zone and the full C_{6v} point symmetry. C_{6v} is generated by $R_{2\pi/3}$, the rotation of the lattice by angle $2\pi/3$ around an empty hexagon, R_π and σ , a reflection whose axis is a diameter of an empty hexagon, and the IRs of C_{6v} are labelled by the associated three quantum numbers $\mathcal{R}_{2\pi/3}, \mathcal{R}_\pi$ and σ . The IRs of T_N are labelled by the \mathbf{k} vector of the first Brillouin zone.

\mathcal{O}	\mathbf{k}	$\mathcal{R}_{2\pi/3}$	σ	ν
A_1	0	1	1	1
A_2	0	1	-1	2
E	0	j, j^2		3
T_1	$\mathbf{X}_{1,2,3}$		-1	4
T_2	$\mathbf{X}_{1,2,3}$		1	5

$\{Id, i\}$	\mathcal{R}_π
Γ_e	1
Γ_o	-1

that acts on the wave function $|cuboc\rangle$ of a *cuboc*-ordered state. The Hilbert space that contains such states is a

12
subspace of $\bigotimes_{i=1}^{12} \mathcal{D}_{N/24}$, where $\mathcal{D}_{N/24}$ is the Hilbert space

of one spin $N/24$. Thus, a natural choice for $\hat{U}(g)$ would be the tensor product of twelve $\hat{U}_{N/24}(g)$ matrices, each one of them representing g in $\mathcal{D}_{N/24}$.

Now we know that in each subspace $\mathcal{D}_{N/24}$, if $N/24$ is half-integer, $\hat{U}_{N/24}(g)$ and $-\hat{U}_{N/24}(g)$ are equally suitable choices and we cannot decide between them other than arbitrarily, due to the double connectedness of $SO(3)$. Let's choose 12 such matrices anyway and form their tensor product $\hat{U}(g)$. When acting on a particular order parameter, named $|cuboc\rangle$, we get

$$\hat{U}(g)|cuboc\rangle = \varphi(g)|cuboc'\rangle \quad (6)$$

where $|cuboc'\rangle$ represents the order parameter obtained by applying the global rotation $g \in \mathcal{O}$ on $|cuboc\rangle$, and $\varphi(g)$ is an overall phase factor that we cannot get rid of since it embeds the arbitrariness of our choice of the matrices $\hat{U}_{N/24}(g)$.

Recall however that $\hat{U}(g)$ acts in a subspace of $\bigotimes_{i=1}^{12} \mathcal{D}_{N/24}$

which is known from spin algebra to contain states with integer spins only, whatever $N/24$, integer or half-integer. Hence $\hat{U}(g)$ is always a true representation of g , *i.e.* no ambiguity should remain in it and consequently nor in $\varphi(g)$. Thus the group law should be exactly verified by $\varphi(g)$ which is then simply a one-dimensionnal, thus irreducible, representation of \mathcal{O} .

Direct computation for $N=12, 24$ and 36 spins indeed shows that $\varphi(g) = \chi_{\nu_0}(g)$, where $\nu_0=1$ for $N=24$ spins, and $\nu_0=2$ for $N=12$ and 36 spins.

Finally, to embed this subtlety in the decomposition (4) one simply has to permute $A_1 \leftrightarrow A_2$ and $T_1 \leftrightarrow T_2$ in Table II for $N=12$ and 36 spins, as can be seen directly on the character table of \mathcal{O} (Table I). Note that no additional ambiguity arises from the consideration of the

$\{Id, i\}$ part of \mathcal{O}_h since the whole discussion relies on the double connectedness of $SO(3)$ which is irrelevant here.

C. Analysis of exact $N=36$ spectrum

We determine the number and degeneracies of the QDJS expected for a sample with $N=36$ spins and compare this to the exact diagonalization result.

We first compute the decomposition (4) for total spin $S \leq 6$, the approximate maximum spin of the QDJS for $N = 36$. As stated earlier we just have to take Table II and perform the relevant permutations $A_1 \leftrightarrow A_2$ and $T_1 \leftrightarrow T_2$. In order to take the whole \mathcal{O}_h group into account we recall that each one of the IRs of the decomposition should actually appear twice with the two possible parities under the spin-flip operation. Then we map these IRs onto those of G_N and here we need to specify the shape of the sample we diagonalize (Fig. 7). The map-

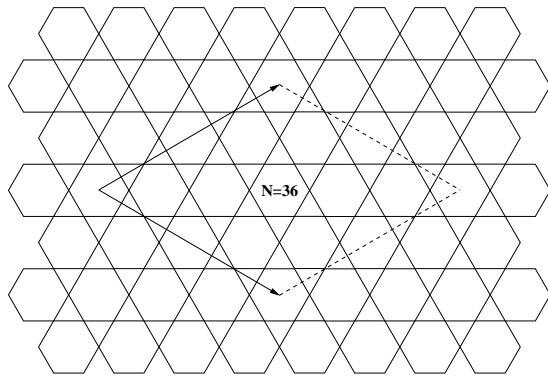


FIG. 7: $N=36$ sample.

ping is readily done since the $N=36$ sample has the full C_{6v} symmetry and we may directly use Table III. Hence we have obtained the full composition of the Anderson's tower of states in the lowest spin sectors $0 \leq S \leq 6$ (Table IV). Again we stress that each QDJS appearing in Table IV should be present twice, with the two parities under the R_π operation, this last result being the hallmark of the \mathbb{Z}_2 symmetry breaking observed classically.

The comparison with the exact spectrum of the Hamiltonian (1) for the $N=36$ sample is straightforward (Fig. 8 and TABLE V). Indeed one clearly notes a set of low energy eigenstates, well separated from the magnon excitations for total spin $S \leq 6$ which scale reasonably as $S(S+1)$. But the main point is that for each total spin S the number and symmetries of the low-lying eigenstates are exactly those obtained from our symmetry analysis, as can be readily verified in TABLE V.

In particular, we note that we have $2(2S+1)$ QDJS in each total spin S sector, consistently with a complete

TABLE IV: Expected symmetries (\mathbf{k} : wave vector, $\mathcal{R}_{2\pi/3}$: phase factor in a lattice $2\pi/3$ rotation, and σ : phase factor in a lattice reflection) and dimensionality (d) of the IRs appearing in the QDJS of the 12-sublattice Néel state. Each of these IRs actually appears twice in the spectra with $\mathcal{R}_\pi = \pm 1$ (not shown), these two copies will be noted in the following e (for even) and o (for odd). The last columns give the number of each IR expected in the S sector (up to $S=6$) for the $N=36$ sample, according to Eq. (5). The last line gives the number $n(S)$ of QDJS in each sector (counting the \mathbb{Z}_2 replica gives a total number of $2n(S)$ QDJS in the spin S sector).

S				0 1 2 3 4 5 6
1	$\mathbf{k} = \mathbf{0}$	$\mathcal{R}_{2\pi/3}=1$	$\sigma = 1$	d=1 0 0 0 1 0 0 1
2	$\mathbf{k} = \mathbf{0}$	$\mathcal{R}_{2\pi/3}=1$	$\sigma = -1$	d=1 1 0 0 0 1 0 1
3	$\mathbf{k} = \mathbf{0}$	$\mathcal{R}_{2\pi/3}=j, j^2$		d=2 0 0 1 0 1 1 1
4	$\mathbf{k} = \mathbf{X}_{1,2,3}$		$\sigma = -1$	d=3 0 0 1 1 1 1 2
5	$\mathbf{k} = \mathbf{X}_{1,2,3}$		$\sigma = 1$	d=3 0 1 0 1 1 2 1
$n(S)$				1 3 5 7 9 11 13

TABLE V: Energies per spin and symmetries of the lowest eigenstates of the Hamiltonian (1) for $S \leq 4$.

S	$E/N J_1 $	IR
0	-0.420920074	2e
0	-0.4200543165	2o
1	-0.4189355373	5o
1	-0.418596983	5e
2	-0.4156541824	3e
2	-0.4153173566	4o
2	-0.4152827263	4e
2	-0.4148859382	3o
3	-0.4105060697	1e
3	-0.410423696	4o
3	-0.4104035497	5o
3	-0.4098987579	4e
3	-0.409886241	5o
3	-0.409738183	1o
4	-0.4041817784	3e
4	-0.4038558602	5e
4	-0.4037970304	2e
4	-0.4035743475	4o
4	-0.4032725096	4e
4	-0.4031726122	5o
4	-0.4029286504	2e
4	-0.4028885961	3o

$SU(2)$ -breaking in the thermodynamic limit, with the factor 2 coming from the two replica $\mathcal{R}_\pi = \pm 1$ of each QDJS and taking care of the \mathbb{Z}_2 symmetry breaking. The same analysis has been made for $N=12$ and 24 non-frustrating samples, leading to the same result.

These symmetry arguments are strong enough to claim that, at least in a certain range of parameters, quantum fluctuations don't destroy the complicated 12-sublattice classical long-range order and that there exists a *quantum cuboc* phase in the thermodynamic limit, in the sense of a ground state consisting of the classical *cuboc* state

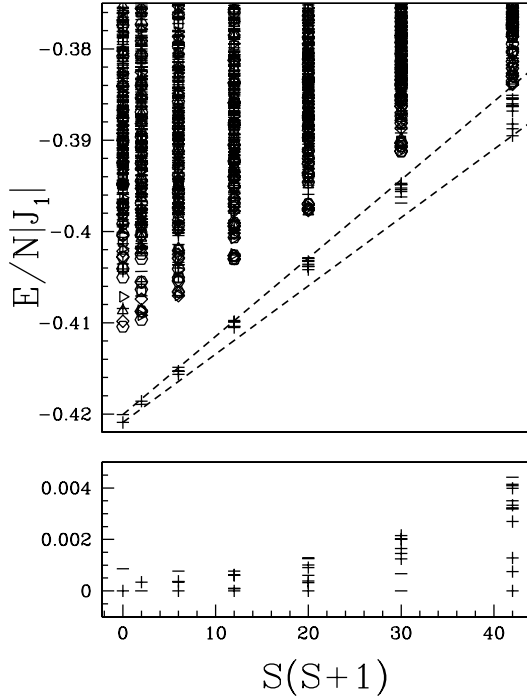


FIG. 8: Top: Exact spectrum of the Hamiltonian (1), with $J_2/|J_1|=0.5$, for the $N=36$ sample shown in Fig. 7. The exact energies per spin are displayed *vs.* $S(S+1)$. The $+$ (resp. $-$) symbols are eigenstates with even (resp. odd) parity under the \mathcal{R}_π lattice rotation. Other symbols are eigenstates without the \mathcal{R}_π symmetry. The full symmetries of the lowest eigenstates are given in Table V. The expected QDJS for the 12-sublattice Néel order appear between the two dashed lines. In particular even and odd parity eigenstates come in equal number in each spin sector as expected for the \mathbb{Z}_2 symmetry breaking. Bottom: Zoom on the QDJS (energies rescaled).

renormalized by quantum fluctuations, as explained earlier.

However, it can be objected that long wavelength quantum fluctuations, which can't be accounted for on the small samples we diagonalized, may wipe out the *cuboc* order.

IV. SEMI-CLASSICAL APPROACH

Now that we are convinced that the 12-sublattice Néel order observed in the classical *cuboc* phase also exists in small samples of spins 1/2, we may compute the effect of long wavelength quantum fluctuations on the energy, sublattice magnetization and chiral order parameter in the ground state using the spin-wave approximation.

The route to compute the quantum deviations to a classical *cuboc* state is straightforward: at each site of the kagomé lattice we define a local frame in spin space whose z-axis is aligned with the local spin in the classical ground state. Thus, in this frame the classical *cuboc* ground state

is simply a ferromagnetic state to which one can readily apply the Holstein-Primakov transformation.

First, we choose a particular *cuboc* state, say the one of Fig. 2. At a given site i of the kagomé lattice we define the local frame $(\mathbf{x}_i, \mathbf{y}_i, \mathbf{z}_i)$ with \mathbf{z}_i the unit vector parallel to the local classical spin \mathbf{S}_i . To choose \mathbf{x}_i we note that each site of the kagomé lattice belongs to two triangles pointing towards opposite directions. Consider the other two spins on the downward triangle and label them j and k with (i,j,k) turning clockwise. The directions of the two spins j,k in our *cuboc* state are \mathbf{z}_j and \mathbf{z}_k and one can easily verify that $\mathbf{x}_i = (\mathbf{z}_k - \mathbf{z}_j)/\sqrt{2}$ is indeed a unit vector orthogonal to \mathbf{z}_i . We completely determine the local frame by imposing $\mathbf{y}_i = \mathbf{z}_i \wedge \mathbf{x}_i$.

This construction is translationally invariant and repeating it for all the sites of the kagomé lattice will lead to 12 different local frames associated to the 12 sublattices of the classical ground state. Hence, using the appropriate transition matrix \mathcal{R}_i from the reference frame $(\mathbf{x}, \mathbf{y}, \mathbf{z})$ to the local frame $(\mathbf{x}_i, \mathbf{y}_i, \mathbf{z}_i)$, we may compute the components of the spin at site i in its local frame $\mathbf{S}'_i = (S_i^{x_i}, S_i^{y_i}, S_i^{z_i})$ from $\mathbf{S}_i = \mathcal{R}_i \mathbf{S}'_i$ (Remark: there are only 12 different \mathcal{R}_i matrices).

Before computing the Hamiltonian (1) in the local frame, we note that it can be rewritten as a sum over the $N/3$ empty hexagons (Fig. 9):

$$\mathcal{H} = J_1 \sum_{\bigcirc} \sum_{\langle i,j \rangle} \mathbf{S}_i \cdot \mathbf{S}_j + J_2 \sum_{\bigcirc} \sum_{\langle\langle i,k \rangle\rangle} \mathbf{S}_i \cdot \mathbf{S}_k \quad (7)$$

where $\langle i,j \rangle$ and $\langle\langle i,k \rangle\rangle$ are now respectively the six nearest and six next-nearest neighbor pairs of sites enclosed in the empty hexagon \bigcirc . Now, using $\mathbf{S}_i \cdot \mathbf{S}_j = \mathbf{S}'_i T_{ij} \mathbf{S}'_j$, with $T_{ij} = {}^t \mathcal{R}_i \mathcal{R}_j$, we may rewrite (7) in the local frame as

$$\mathcal{H} = J_1 \sum_{\bigcirc} \sum_{\langle i,j \rangle} \mathbf{S}'_i T_{ij} \mathbf{S}'_j + J_2 \sum_{\bigcirc} \sum_{\langle\langle i,k \rangle\rangle} \mathbf{S}'_i T_{ik} \mathbf{S}'_k \quad (8)$$

Now, we are able to quantize the fluctuations around the classical *cuboc* state using Holstein-Primakov bosons. Up to quadratic order the transformation at site i writes

$$\begin{cases} S'_i^+ = S_i^{x_i} + j S_i^{y_i} = \sqrt{2S-n_i} c_i \simeq \sqrt{2S} c_i \\ S'_i^- = S_i^{x_i} - j S_i^{y_i} = \sqrt{2S-n_i} c_i^\dagger \simeq \sqrt{2S} c_i^\dagger \\ S'_i^z = S_i^{z_i} = S - n_i \end{cases} \quad (9)$$

where c_i^\dagger and c_i respectively create and annihilate an Holstein-Primakov boson at site i , with S the length of the classical local spin and $n_i = c_i^\dagger c_i$.

Inserting (9) into (8) we obtain the quantized version of the original Hamiltonian (1) up to quadratic order. As usual we Fourier-transform c_i and c_i^\dagger according to

$$c_i = \sqrt{\frac{3}{N}} \sum_{\mathbf{q}} e^{-i\mathbf{q} \cdot (\mathbf{R}_{\bigcirc} + \mathbf{e}_{\mu_i})} c_{\mathbf{q}}^{\mu_i} \quad (10)$$

where the sum runs over the first Brillouin zone, \mathbf{R}_{\bigcirc} is a vector of the Bravais lattice and $\mu_i = \alpha, \beta, \gamma$ indicates

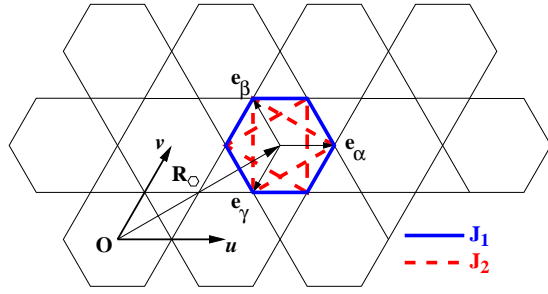


FIG. 9: (Color online) Kagomé lattice with nearest (solid) and next-nearest neighbor exchange (dashed). Note that we span all the exchange paths by considering the 12 links inside an empty hexagon \circ located at \mathbf{R}_\circ and then iterate over the whole Bravais lattice. \mathbf{u} and \mathbf{v} are the basis vectors of the Bravais lattice of length 2 and the three sites α, β, γ per Bravais cell define the three unit vectors $\mathbf{e}_\alpha = \mathbf{u}/2$, $\mathbf{e}_\beta = (\mathbf{v} - \mathbf{u})/2$ and $\mathbf{e}_\gamma = -\mathbf{v}/2$.

one of the three possible sites in the Bravais cell (Fig. 9). Again, in the local frame the complicated twelve sublattice order is just a ferromagnetic state, so that we need only three flavors of bosons $\mu_i = \alpha, \beta, \gamma$ associated to the three sites per Bravais cell on the kagomé lattice. We may finally bring the Hamiltonian to matrix form as

$$\mathcal{H} = (J_1 - J_2)NS(S+1) + \sum_{\mathbf{q}} V_{\mathbf{q}}^\dagger M_{\mathbf{q}} V_{\mathbf{q}} \quad (11)$$

where the sum runs over the entire first Brillouin zone, $V_{\mathbf{q}}$ is the column vector $(c_{\mathbf{q}}^\alpha, c_{\mathbf{q}}^\beta, c_{\mathbf{q}}^\gamma, c_{-\mathbf{q}}^{\alpha\dagger}, c_{-\mathbf{q}}^{\beta\dagger}, c_{-\mathbf{q}}^{\gamma\dagger})$, and $M_{\mathbf{q}}$ is the 6×6 matrix $M_{\mathbf{q}} = (J_2 - J_1)S\mathbb{1} + \begin{pmatrix} A_{\mathbf{q}} & B_{\mathbf{q}} \\ B_{-\mathbf{q}} & A_{-\mathbf{q}} \end{pmatrix}$ with $\mathbb{1}$ the identity matrix, and

$$A_{\mathbf{q}} = \begin{pmatrix} 0 & a_{\alpha\beta}(\mathbf{q}) & a_{\alpha\gamma}(\mathbf{q}) \\ a_{\alpha\beta}(\mathbf{q}) & 0 & a_{\beta\gamma}(\mathbf{q}) \\ a_{\alpha\gamma}(\mathbf{q}) & a_{\beta\gamma}(\mathbf{q}) & 0 \end{pmatrix} \quad (12)$$

and

$$B_{\mathbf{q}} = \begin{pmatrix} 0 & b_{\alpha\beta}(\mathbf{q}) & b_{\alpha\gamma}(\mathbf{q}) \\ b_{\alpha\beta}(-\mathbf{q}) & 0 & b_{\beta\gamma}(\mathbf{q}) \\ b_{\alpha\gamma}(-\mathbf{q}) & b_{\beta\gamma}(-\mathbf{q}) & 0 \end{pmatrix} \quad (13)$$

with

$$\begin{aligned} a_{\alpha\beta}(\mathbf{q}) &= \frac{J_2 S}{4} \cos q_{\beta-\alpha} - \frac{J_1 S}{4} \cos q_\gamma - \frac{J_1 S}{\sqrt{2}} \sin q_\gamma \\ b_{\alpha\beta}(\mathbf{q}) &= \frac{J_2 S}{4} \cos q_{\beta-\alpha} - \frac{J_1 S}{4} \cos q_\gamma + \frac{J_2 S}{\sqrt{2}} \sin q_{\beta-\alpha} \end{aligned}$$

with the four remaining matrix elements obtained by cyclic permutation of the indices and where we have used the condensed notation $q_{\beta-\alpha} = \mathbf{q} \cdot (\mathbf{e}_\beta - \mathbf{e}_\alpha)$.

Note that the first term in (11) contains the usual dominant contribution to the renormalization of the classical ground state energy $(J_1 - J_2)NS^2$. Note also that

$A_{\mathbf{q}}^\dagger = A_{\mathbf{q}}$ and $B_{\mathbf{q}}^\dagger = B_{-\mathbf{q}}$ so that $M_{\mathbf{q}}$ is indeed hermitic. As usual the next step is to find a transition matrix $P_{\mathbf{q}}$ such as $M_{\mathbf{q}}$ is diagonal in the new basis.

It should be emphasized that $P_{\mathbf{q}}$ is strongly prescribed by the fact that it has to preserve the boson commutation relations²⁴, much in the same way as the Bogoliubov transformation for the collinear antiferromagnet on the square lattice.

We end up with three Bogoliubov bosons, obtained from $W_{\mathbf{q}} = (d_{\mathbf{q}}^\alpha, d_{\mathbf{q}}^\beta, d_{\mathbf{q}}^\gamma, d_{-\mathbf{q}}^{\alpha\dagger}, d_{-\mathbf{q}}^{\beta\dagger}, d_{-\mathbf{q}}^{\gamma\dagger}) = P_{\mathbf{q}} V_{\mathbf{q}}$, and the six eigenvalues give the corresponding three dispersion branches.

In the new basis (11) reads:

$$\mathcal{H} = (J_1 - J_2)NS(S+1) + \sum_{\mathbf{q}} \sum_{\mu=\alpha,\beta,\gamma} \omega_{\mathbf{q}}^\mu (d_{\mathbf{q}}^{\mu\dagger} d_{\mathbf{q}}^\mu + \frac{1}{2}) \quad (14)$$

so that the energy per spin in the ground state, which is the vacuum $|0\rangle$ of $d_{\mathbf{q}}^\mu$ Bogoliubov bosons, is simply:

$$e_0^N = \frac{1}{N} \langle 0 | \mathcal{H} | 0 \rangle = (J_1 - J_2)S(S+1) + \frac{1}{2N} \sum_{\mathbf{q}} \sum_{\mu=\alpha,\beta,\gamma} \omega_{\mathbf{q}}^\mu \quad (15)$$

As for the collinear antiferromagnet, note that the Bogoliubov transformation $P_{\mathbf{q}}$ is actually singular whenever $\omega_{\mathbf{q}}^\mu = 0$, namely at $\mathbf{q} = \mathbf{X}_{1,2,3}$ where soft modes are expected in the thermodynamic limit. One indeed verifies that the lowest branch vanishes at each one of the three edge centers of the first Brillouin zone giving exactly three Goldstone modes in the thermodynamic limit, as expected for a complete $SU(2)$ symmetry breaking. We may then compute the renormalization of the magnetization in the local basis

$$m^N = \frac{1}{NS} \langle 0 | \sum_{i=1}^N S_i^{z_i} | 0 \rangle = 1 + \frac{1}{S} \left(1 - \frac{1}{N} \sum'_{\mathbf{q}} \sum_{i,j=1}^3 (P_{\mathbf{q}}^{i,j})^2 \right) \quad (16)$$

where the prime denotes a sum over the first Brillouin zone deprived of its three edge centers and where $P_{\mathbf{q}}^{i,j}$ is the $(i,j)^{th}$ matrix element of the matrix $P_{\mathbf{q}}$.

Another quantity of interest to us is the renormalization of the scalar chirality on a triangle. It is naturally normalised by its value in the classical ground state, so that we define $\xi_\Delta = \frac{\sqrt{2}}{S^3} (\mathbf{S}_i \wedge \mathbf{S}_j) \cdot \mathbf{S}_k$ on each triangle (i,j,k) , with (i,j,k) turning clockwise. We may then compute the renormalisation of the alternate scalar chirality in the ground state as

$$m_\xi^N = \frac{3}{2N} \langle 0 | \sum_\Delta (-1)^{\alpha_\Delta} \xi_\Delta | 0 \rangle = 1 + \frac{3}{S} \left(1 - \frac{1}{N} \sum'_{\mathbf{q}} \mathcal{D}_{\mathbf{q}} \right) \quad (17)$$

where the sum runs over the $2N/3$ triangles of the kagomé lattice, while α_Δ is respectively 0 and 1 on upward and

downward triangles, and

$$\mathcal{D}_q = \sum_{i,j=1}^3 (P_q^{i,j})^2 - \frac{1}{2} \sum_{j=1}^3 \left(\begin{array}{l} \cos q_\alpha (P_q^{2,j} + P_q^{5,j})(P_q^{3,j} + P_q^{6,j}) \\ + \cos q_\beta (P_q^{1,j} + P_q^{4,j})(P_q^{3,j} + P_q^{6,j}) \\ + \cos q_\gamma (P_q^{1,j} + P_q^{4,j})(P_q^{2,j} + P_q^{5,j}) \\ + \frac{\sqrt{2}}{3} \sin q_\alpha (P_q^{5,j} P_q^{6,j} - P_q^{2,j} P_q^{3,j}) \\ + \frac{\sqrt{2}}{3} \sin q_\beta (P_q^{4,j} P_q^{6,j} - P_q^{1,j} P_q^{3,j}) \\ + \frac{\sqrt{2}}{3} \sin q_\gamma (P_q^{4,j} P_q^{5,j} - P_q^{1,j} P_q^{2,j}) \end{array} \right) \quad (18)$$

These quantities were numerically computed on finite size samples with linear sizes $L \leq 10^2$ Bravais lattice spacings. As usual the leading correction to the classical value comes from the first magnon excitation whose energy scales as $1/L$. We find very good agreement with the expected scaling laws for e_0^N ($\sim 1/L^3$), m^N ($\sim 1/L$) and m_ξ^N ($\sim 1/L$), and perform the extrapolation to the thermodynamic limit.

We first note in (Fig. 10) that in the thermodynamic limit m^∞ and m_ξ^∞ remain finite in a large region around the point where exact diagonalizations were performed, thus showing the stability of the *cuboc* phase against long wavelength quantum fluctuations. For $J_2/|J_1| = 0.5$ we find to lowest order in the spin wave approximation that m^∞ and m_ξ^∞ are renormalized by 16% and 50% respectively.

However, upon increasing J_2 , both quantities decrease drastically. For $J_2/|J_1| \gtrsim 3$ the chirality disappears which casts a strong doubt on the stability of the 12-sublattice state itself in this range of parameters.

V. A GAPPED PHASE FOR $J_2/|J_1| = 5.0$

Exact spectra for $J_2/|J_1| = 5.0$ differ notably from spectra of an ordered phase as described in section III. First of all, their low lying levels in each S sector do not scale as $S(S+1)$ but rather as S as can be seen in Fig. 11. Second the gap to the first excitation seemingly does not close to zero with the system size as shown in Fig. 12. This second result is consistent with the first one: in a gapped phase a finite magnetic field H_c is needed to close the gap. This critical field is directly proportional to the first derivative of the energy versus S . For this given model in this range of parameters, the available sizes of exact spectra are large enough to infirm the presence of a twelve sub-lattice Néel order and confirm the existence of a gapped phase. They are not large enough to discriminate between a true Spin Liquid or a Valence Bond Crystal, and to decide if there is one or two different gapped phases in this range of parameter.

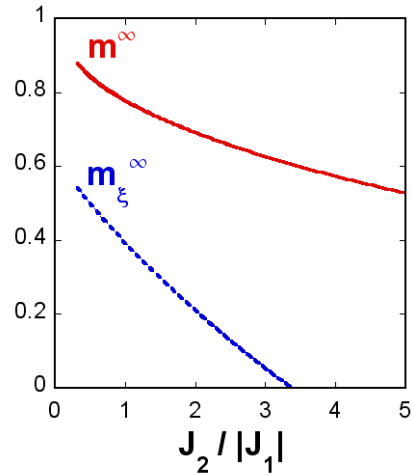


FIG. 10: (Color online) Extrapolated values of the magnetization in the local basis m^∞ (solid line) and the alternate scalar chirality m_ξ^∞ (dashed line) as a function of $J_2/|J_1|$.

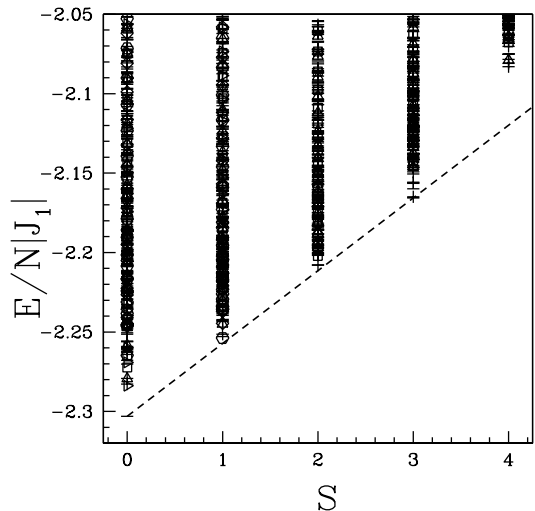


FIG. 11: Exact spectrum of the $N=36$ sample for $J_2/|J_1|=5.0$ vs. total spin S . The symbol convention is the same as that of Fig. 8.

VI. CONCLUSION

In this paper we have studied the $J_1 - J_2$ model on the kagomé lattice, for $J_1 < 0$ and $J_2 > 0$. We have found a 12-sublattice ordered phase for $J_1 < 0$ and $J_2/|J_1| > 1/3$. This new phase was shown to resist quantum fluctuations. On exact spectra of small size samples, we found the complete signature of this complicated Néel order, *i.e.* the number and symmetries of the QDJS in the tower of states, based on a very general group-theoretical approach. Moreover, in the spin wave approximation, long wavelength quantum fluctuations were found to renormalize the order parameter to a finite value in a finite

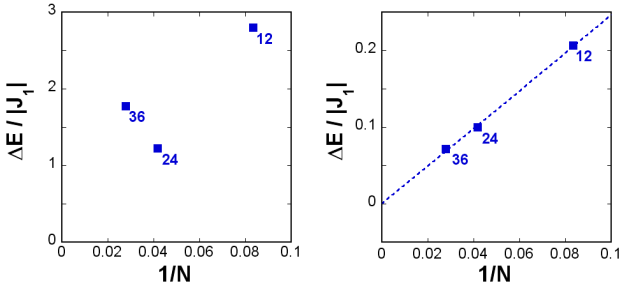


FIG. 12: (Color online) Left: Finite size scaling of the spin gap ΔE for $J_2/|J_1| = 5.0$, in the supposed to be gapped phase. Right: The same gap in the 12-sublattice Néel phase, for $J_2/|J_1| = 0.5$, closes as $1/N$ as expected for the à la Néel $SU(2)$ symmetry breaking (section III A).

range of parameters up to $J_2/|J_1| \simeq 3$.

The non-coplanarity of the 12 sublattices in the *cuboc* phase was shown to induce a chiral symmetry breaking, to which we associated a chiral order parameter. Classically, we showed that this \mathbb{Z}_2 symmetry was restored at finite temperature, consistently with the Mermin-Wagner theorem, though the exact nature of the transition remains to be investigated. We were also able to find the signature of this discrete symmetry breaking on exact spectra.

Finally, we showed in the spin-wave approach that the 12 sublattice order is wiped out by quantum fluctuations for $J_2/|J_1| \gtrsim 3$. Exact diagonalisations indeed confirm the existence of a spin-gap phase, with short range order in spin-spin correlations. For this model the largest available sizes ($N = 36$) are too small to give more information on the nature of this quantum phase.

Laboratoire de Physique Théorique de la Matière Condensée is UMR 7600 of CNRS.

- * Electronic address: jcdomeng@lptl.jussieu.fr
- ¹ V. Elser, Phys. Rev. Lett. **62**, 2405 (1989).
- ² J. T. Chalker, P. C. W. Holdsworth, and E. F. Shender, Phys. Rev. Lett. **68**, 855 (1992).
- ³ P. Lecheminant, B. Bernu, C. Lhuillier, L. Pierre, and P. Sindzingre, Phys. Rev. B **56**, 2521 (1997).
- ⁴ C. Waldtmann, H. Everts, B. Bernu, C. Lhuillier, P. Sindzingre, P. Lecheminant, and L. Pierre, Eur. Phys. J. B **2**, 501 (1998).
- ⁵ R. Budnik and A. Auerbach, Phys. Rev. Lett. **93**, 187205 (2004).
- ⁶ G. Misguich and C. Lhuillier, *Two-dimensional quantum antiferromagnets* (World-Scientific, Singapore, 2005), cond-mat/0310405.
- ⁷ A. B. Harris, C. Kallin, and A. J. Berlinsky, Phys. Rev. B **45**, 2899 (1992).
- ⁸ M. Elhajal, B. Canals, and C. Lacroix, Phys. Rev. B **66**, 014422 (2002).
- ⁹ C. Waldtmann, Ph.D. thesis, Hannover (2000).
- ¹⁰ A. P. Ramirez, Annu. Rev. Mater. Sci **24**, 453 (1994), and references therein.
- ¹¹ A. P. Ramirez, B. Hessen, and M. Winklemann, Phys. Rev. Lett. **84**, 2957 (2000).
- ¹² P. Mendels, A. Keren, L. Limot, M. Mekata, G. Collin, and M. Horvatic, Phys. Rev. Lett. **85**, 3496 (2000).
- ¹³ D. Bono, P. Mendels, G. Collin, N. Blanchard, F. Bert, A. Amato, C. Baines, and A. D. Hillier, Phys. Rev. Lett. **93**, 187201 (2004).
- ¹⁴ Z. Hiroi, M. Hanawa, N. Kobayashi, M. Nohara, H. Takagi, Y. Kato, and M. Takigawa, J. Phys. Soc. Jpn **70**, 3377 (2001).

- ¹⁵ H. Kageyama, T. Nakajima, M. Ichihara, F. Sakai, and Y. Ueda, *Spin frustration in two-dimensional compounds* (Kyushu University Press, Fukuoka, Japan, 2002), p. 135, ISBN 4 87378 740 8.
- ¹⁶ P. Millet, B. Bastide, V. Pashchenko, S. Gnatchenko, V. Gapon, Y. Ksari, and A. Stepanov, Journal of Materials Chemistry **11**, 1152 (2001).
- ¹⁷ Y. Narumi, K. Katsumata, Z. Honda, J.-C. Domenge, P. Sindzingre, C. Lhuillier, Y. Shimaoka, T. Kobayashi, and K. Kindo, Europhys. Lett. **65** (5), 705 (2004).
- ¹⁸ B. Delamotte, D. Mouhanna, and M. Tissier, Phys. Rev. B **69**, 134413 (2004).
- ¹⁹ J.-C. Domenge, C. Lhuillier, and P. Viot (2005), in preparation.
- ²⁰ B. Bernu, C. Lhuillier, and L. Pierre, Phys. Rev. Lett. **69**, 2590 (1992).
- ²¹ B. Bernu, P. Lecheminant, C. Lhuillier, and L. Pierre, Phys. Rev. B **50**, 10048 (1994).
- ²² O. Waldmann, to be published in Coord. Chem. Rev. (2005).
- ²³ P. Anderson, Mater. Res. Bull. **8**, 153 (1973).
- ²⁴ J. Colpa, Physica A **93**, 327 (1978).

²⁵ In our problem the representation space is $\mathcal{E} = \bigotimes_{i=1}^{12} \mathcal{D}_{N/24}$.

For large values of S the subspace of \mathcal{E} with total spin S has a dimension smaller than $2S + 1$ and can only display a limited set of the states appearing in the decomposition (4). However, at least up to $S < \sqrt{N}$, it can be verified by direct inspection that the number of states in \mathcal{E} with total spin S is much larger than $(2S + 1)$.